Journal of CO_2 Utilization 40 (2020) 101228

Contents lists available at ScienceDirect

Journal of CO_2 Utilization

journal homepage: www.elsevier.com/locate/jcou

CO_2 methanation process synthesis by superstructure optimization

Jennifer Uebbing[a,b], Liisa Rihko-Struckmann[a,*], Sebastian Sager[b], Kai Sundmacher[a,c]

[a] Process Systems Engineering, Max Planck Institute for Dynamics of Complex Technical Systems, Sandtorstrasse 1, 39106 Magdeburg, Germany
[b] Institute of Mathematical Optimization, Faculty of Mathematics, Otto-von-Guericke University Magdeburg, Germany
[c] Institute of Process Engineering, Faculty of Process- and Systems Engineering, Otto-von-Guericke University Magdeburg, Germany

ARTICLE INFO

Keywords:
Power-to-methane
Superstructure
MINLP
Global optimization
CAPEX
Energy efficiency

ABSTRACT

A superstructure optimization approach to power-to-methane process design that includes heat integration is presented. Carbon dioxide from biogas plants is considered as carbon source. The superstructure includes 13 alternative process technologies in seven layers for power-to-methane processes at their current stage of development. For different scenarios, the most efficient process in terms of product chemical exergy and the most cost-effective process in terms of capital and total annual costs are identified. We consider indirect heat integration via utilities, which for all scenarios, is determined to be a main contributor to both energy efficiency and process cost. The product methane must meet the requirements for feed into the gas grid. The requirements for the gas grid have a direct influence on the most efficient process route. The number of necessary process units is reduced, if hydrogen can be fed to the gas grid. Furthermore, extend of the heat exchanger network determines the trade-off between efficiency and costs, rather than choice of unit operations.

1. Introduction

While the share of electrical energy generated from volatile energy sources, such as wind and sun, in the power grid is constantly growing, the need for efficient energy storage remains. In particular, the long-term storage of electrical energy is still a great challenge. Promising alternatives for long-term storage include pumped hydro-storage and power-to-liquid and power-to-gas storage technologies [1]. Power-to-gas, particularly power-to-methane, has been shown to be necessary, if a complete transition to renewable energy is to take place [1,2]. Methane as an energy carrier has the advantage of an existing infrastructure for storage and transportation – the natural gas grid, as well as a higher energy storage capability than methanol [3]. Furthermore, synthetic natural gas (SNG) can substitute for natural gas from fossil resources seamlessly, making the adaptation of the end user unnecessary. Nonetheless, low efficiency and high costs are significant challenges to be tackled. The economic feasibility of the process still strongly depends on the price of electricity for water electrolysis [4]. The technology is currently in the pilot or demonstration stage, and many different process alternatives are considered. Extensive lists of pilot and demonstration plants can be found, e.g., in recent reviews by Götz et al. [5], Bailera et al. [6], and Rönsch et al. [7].

Power-to-methane denotes the production of methane from hydrogen from water electrolysis and carbon dioxide. The exothermic reaction

$$CO_2 + 4H_2 \rightleftharpoons CH_4 + 2H_2O, \quad \Delta H^0 = -165\ \text{kJ/mol} \tag{1}$$

is implemented via a catalytic or biological methanation reactor. Nickel-alumina catalysts are commonly used for the catalytic methanation in a fixed bed reactor. While other materials have higher selectivity (platinum) or activity (ruthenium, iron) than nickel [7], nickel-alumina catalysts are preferred in practice because of the low costs. The range of operation of nickel-aluminium catalysts is below 15 bar, between 425 and 975 K [6], however, in practice temperatures of 450–700 K and pressures below 8 bar are often preferred [6,8]. The biological methanation by methanogenic bacteria is an alternative for the thermo-chemical conversion. A wide range of methanogens are currently researched for biological methanation. Most studies consider methanation at ambient pressure and temperatures from 308 to 370 K [9,10]. Because of the variations in type of methanogens, reactor construction, feed, and gas transfer rates in the studies, there is a large range of reported conversion rates in biological methanation [5,11,12].

An important aspect of the power-to-methane process is the carbon source. CO_2 is often considered as its reuse reduces carbon mitigation to the atmosphere. Next to flue gas from industrial processes, such as those from the cement industry or power plants [13], CO_2 can be gained from biogas plants. The latter is a very promising source insofar as infrastructure exists on-site, i.e., a connection to the gas grid for the

* Corresponding author.
E-mail address: rihko@mpi-magdeburg-mpg.de (L. Rihko-Struckmann).

https://doi.org/10.1016/j.jcou.2020.101228

Available online 18 July 2020
2212-9820/ © 2020 The Authors. Published by Elsevier Ltd. This is an open access article under the CC BY license (http://creativecommons.org/licenses/BY/4.0/).

separated methane. Biogas has the advantage over flue gas in that less purification is required to further the processing of the gas via methanation. Witte et al. [14] have shown recently that, in practice, only the separation of sulfur components is necessary to avoid methanation catalyst degradation. Nonetheless, the question arises whether the mixture should be supplied to the reactor directly or if prior separation of CH_4 and CO_2 is necessary to increase the methane yield in the subsequent methanation unit. The range of technologies for the separation of CH_4 and CO_2 is wide. Absorption, adsorption, and membrane separation have been extensively applied in industry [15].

Another important issue is the choice of electrolyzer for hydrogen supply. Alkaline electrolyzers (AE) are established technologies and commercially available. However, high-temperature electrolysis (SOEC) could improve process efficiency by utilizing the excess heat released by the exothermic methanation reaction [16]. Jeanmonod et al. [17] recently showed that the use of SOEC for co-electrolysis shows promising results for power-to-methane processes.

The aim of this study is to identify promising combinations of these technologies via superstructure optimization at the steady state operating conditions.

We focus on optimization of thermo-economic aspects of the process alternatives via exergy efficiency, capital costs and total annual costs. Exergy analysis allows us to combine the different forms energy, in terms of electrical energy, heat, and the energy stored in forms of chemical energy carriers, to a unified term. The exergy value expresses the amount of energy, which is thermodynamically convertible to work. In case of electrical energy the exergetic value is equal to the energetic value. Heat and chemical exergy, however, are determined in relation to a given environment [18,19]

Superstructure optimization is a powerful tool for determining the optimal process configuration from a large variety of technologies and their respective combinations. As heat integration plays an important role in improving the process efficiency, we further include indirect, simultaneous heat integration via pinch analysis in the superstructure model.

Superstructures have been widely applied in systems engineering and process design. They are applied for designing heat exchanger networks [20,pp.111], [21,22], distillation columns [23], optimization of process flowsheets [24], and process synthesis [25]. Further applications can be found in the excellent reviews of Chen and Grossmann [26] and Trespalacios and Grossmann [27]. As most of the above examples, we formulate the superstructure as a mixed-integer non-linear problem (MINLP). MINLPs combine the difficulties of non-linear optimization problems (NLP) and mixed-integer linear problems (MILP), which also belong to the class of NP-hard problems. Consequently, solving MINLPs is challenging, and runtimes grow rapidly in the problem dimension. Nonetheless, deterministic, global solvers exist today, such as Baron [28] or the Solving Constraint Integer Programs (SCIP) solver [29], which we applied here. SCIP is a state-of-the-art branch-and-bound solver, with extensive presolving. In the numerical analysis carried out by Kronqvist [30], the solver SCIP showed performance comparative to the commercial solver Baron for convex problems. As an open-source software, SCIP has the advantage over commercial solvers of being easily extendable by the user.

The key novelty of the current work is a detailed designed superstructure for the power-to-methane process, which includes the most relevant unit operations for catalytic CO_2 methanation and additionally simultaneous heat integration. The numerical results represent the global optimal value of the optimization problem as determined by the deterministic global optimization solver SCIP. The optimization of the resulting MINLP model allows for an exhaustive technical analysis of a large variety of possible process configurations (Fig. 1).

We describe the superstructure model, including the individual unit models, in Section 2. The objectives of the superstructure optimization are maximizing process efficiency and minimizing investment costs, as addressed in detail in Section 2.2. We introduce different case studies in Section 3 and show the respective optimization results.

2. Modeling

To derive the process superstructure model, we introduce two levels of modeling: On the unit level we describe the behavior of a single process unit mathematically, e.g., the temperature dependence of a chemical reactor. We introduce the models used for the power-to-methane process in Section 2.1. On the next modeling level, the individual unit models are combined into the superstructure model, which is introduced in Section 2.2.

2.1. Unit models

Unit level models represent the behavior of single-process units in terms of material and energy balances. The scheme of a unit model U is shown in Fig. 2.

We formally define a unit model U as

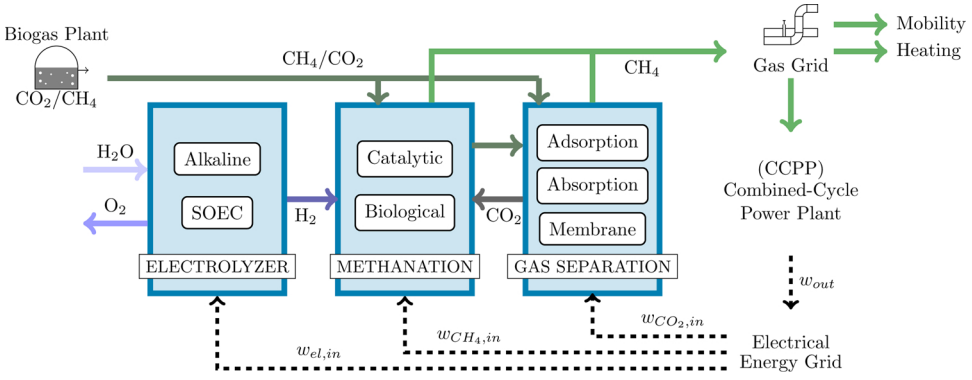

Fig. 1. Schematic overview of the process boundaries. Biogas is a CO_2/CH_4 gas mixture obtained by anaerobic digestion of organic biomass. It is dried and purified from sulfur components, e.g. via activated carbon filters, prior to entering the process under ambient conditions. The biogas mixture can be separated into methane, which is fed to the gas grid, and carbon dioxide, which is fed to the methanation reactor. Alternatively, the mixture can directly be fed to the methanation reactor. For the conversion of CO_2 to CH_4 we consider a large variety of electrolysis, methanation and separation technologies. The final product must be clean enough to be fed into the gas grid, i.e. fulfill the specifications given by the local distribution company and national laws.

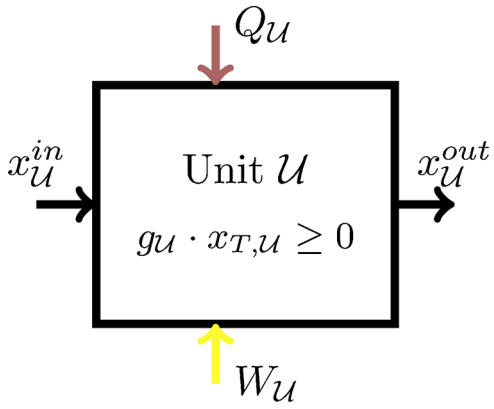

Fig. 2. Scheme of a process unit model. A unit model consists of in- and outgoing material streams, here denoted x_{in} and x_{out}. Furthermore, energy is supplied to or produced by the unit in form of work W_U (only supplied to) and heat Q_U. The individual unit behavior is modeled by constraints g_U.

$x_U \in \mathbb{R}^{n_U}$	variables
$x_U^{\text{in}} \in \mathbb{R}^{m \times d_U^{\text{in}}}$	unit input material stream
$g_U(x_U, x_U^{\text{in}}) \leq 0$	unit inequality constraints
$h_U(x_U, x_U^{\text{in}}) = 0$	unit equality constraints
$\text{lb}_U \leq x_U \leq \text{ub}_U$	box constraints
$x_U^{\text{out}}(x_U, x_U^{\text{in}})$: $\mathbb{R}^{n_U} \times \mathbb{R}^{m \times d_U^{\text{in}}} \to \mathbb{R}^{m \times d_U^{\text{out}}}$	map to unit output material stream
$W_U(x_U)$: $\mathbb{R}^{n_U} \to \mathbb{R}^+$	work demand
$Q_U(x_U)$: $\mathbb{R}^{n_U} \to \mathbb{R}^{n_q}$	heat demand/surplus
$\text{CAPEX}_U(x_U)$: $\mathbb{R}^{n_U} \to$	investment cost
$d_U^{\text{in}}, d_U^{\text{out}} \in \mathbb{N}$	number of in − and outgoing material streams
$m \in \mathbb{N}$	dimension of a single material stream

A uniform formulation of all unit models enables the connection of individual models to a superstructure.

Material streams are sets of variables that represent physical properties of the material flow entering or leaving a unit. In the superstructure model, these variables are shared between connected unit models. The dimension of material streams m is equal for all considered unit models, to allow for the connection of arbitrary models. The number of in- and outgoing material streams is specific to a unit. For example, separation units have typically $d_U^{\text{out}} = 2$ outgoing material streams, whereas for a reactor, $d_U^{\text{out}} = 1$ holds. The information passed to a subsequent unit are molar flows N, temperature T, and pressure p. In the following, the molar gas flow rates are indicated by the variable N, and the subscript indicates the component, respectively, e.g. N_{H_2} indicates the molar gas flow rate of hydrogen. For example, an input stream to unit l takes the form $x_U^{\text{in},l} = [N_{CO_2}^{\text{in},l}, N_{H_2}^{\text{in},l}, N_{CH_4}^{\text{in},l}, N_{H_2O}^{\text{in},l}, T^{\text{in},l}, p^{\text{in},l}]$, thus, for the dimension of the material stream $m = 6$ holds.

Below, the individual unit models are introduced. Here, we drop the subscript U to increase simplicity and readability. We include it again in the superstructure description in Section 2.2.

2.1.1. Electrolysis

For the electrolyzer, we consider two different technologies: AE and solid oxide electrolyzer cells (SOEC). AE is a mature technology that is largely available commercially. We implemented AE as a simplified black box model assuming the electrical energy demand to be linearly dependent on the produced H_2 amount according to

$$W(x) = w_{\text{AE}} \cdot N_{H_2}^{\text{out}}$$

with $w_{\text{AE}} = 378.9$ [31].

As an alternative, we consider the SOEC. The technology is not yet fully mature for industrial application on larger scales. However, SOEC is of high interest, owing its high efficiency and heat-integration potential. We calculate the electrical energy demand W for SOEC from the value of 3.37 kWh/m^3 given by Gruber et al. [32] corresponding to 269.9 kJ/mol$_{H_2}$. In addition, high temperature electrolysis at $T = 1173$ K has a heat demand of 66 kJ/mol$_{H_2}$ and a heat production caused by the stack overpotential of 87 kJ/mol$_{H_2}$, resulting in an external excess heat of 21 kJ/mol$_{H_2}$. Furthermore, the heat demand for the preheating and vaporization of water is considered. We scale the process to 1 MW electrical energy for water electrolysis, with 2.64 mol$_{H_2}$/s (AE) or 3.71 mol$_{H_2}$/s (SOEC) entering the methanation process. We use the corresponding stoichiometric amount of 0.66 mol$_{CO_2}$/s (AE) or 0.93 mol$_{CO_2}$/s (SOEC) in the feed gas from anaerobic digestion as a reference for a priori size estimations of the biological methanation reactor, black box separation models.

2.1.2. Catalytic methanation reactor

To model the reaction in a catalytic methanation reactor, we allow conversion up to thermodynamic equilibrium under isothermal conditions. The output molar flow rates N_i are constrained by thermodynamic equilibrium according to

$$p_{CO_2} p_{H_2}^4 K_{\text{eq}}(T^{\text{in}}) \leq p_{H_2O}^2 p_{CH_4} \quad \text{with } p_i = p^{\text{in}} \frac{N_i}{\sum_{j \in C} N_j}$$

where N_i denotes the molar flow rate in mol/s and p_i is the partial pressure of component $i \in C = \{CO_2, H_2, H_2O, CH_4\}$. In addition the reaction stoichiometry

$$N_i - (\zeta \nu_i + N_i^{\text{in}}) = 0 \quad \text{for } i \in C$$

must hold, where ζ denotes the extend of reaction and ν_i the stoichiometric coefficient of component i. The reaction is highly exothermic. Consequently, the isothermally operating methanation unit creates excess heat. The heat of reaction ΔH_{rxn} is linearly approximated over the relevant temperature interval.

$$\begin{aligned} x^{\text{out}}(x, x^{\text{in}}) &= [N_{CO_2}, N_{H_2}, N_{CH_4}, N_{H_2O}, T^{\text{in}}, p^{\text{in}}] \\ W(x) &= 0 \\ Q(x) &= -\zeta \Delta H_{\text{rxn}} \end{aligned}$$

During the superstructure optimization the pressure of the methanation reactor was fixed to 0.6 MPa, and the temperature was allowed to vary in the range of 580–650 K. These conditions are typically applied for heterogeneously catalyzed methanation reactors [33,34,8].

Investment cost is estimated based on equipment sizing via the Guthrie relation [35]. The Guthrie equation is used to estimate the unit capital cost via size and cost of a known reference unit. We estimate the reactor costs without heat exchange by equations given for pressure vessels. A unit of height L_0 and diameter D_0 is used as reference to estimate the unit cost from reference cost C_0 via

$$C = \text{MFCE}\ C_0 \left(\frac{L}{L_0}\right)^{\alpha} \left(\frac{D}{D_0}\right)^{\beta}. \tag{2}$$

The parameter CE corresponds to the CE index, which updates prices to account for inflation. We use the reference value given by Biegler et al. [35] for the cost estimation. To adapt these values to recent 2017 prices, the parameter CE has a value of $\text{CE} = \frac{\text{CEPCI}_{2017}}{\text{CEPCI}_{\text{ref}}} = \frac{558.3}{115}$. Furthermore, the price must is updated with material and pressure factors MF = 1.15 [35]. Finally, we include the cost of the catalyst C_{cat}.

$$\text{CAPEX}(x) = \text{MFCE}\, C_0 \left(\frac{L}{L_0}\right)^{\alpha} \left(\frac{D}{D_0}\right)^{\beta} + C_{\text{cat}} \tag{3}$$

Parameters for (3) were taken from Biegler et al. [35] as $C_0 = 690$\$, $L_0 = 1.22$ m, $D_0 = 0.91$ m, $a = 0.78$, $b = 0.98$. We assume the reactor to be a bundle reactor with 100 pipes with $L = 1.26$ m and $D = 0.02$ m,

containing a total of 56 kg of catalyst. The price is estimated from commercial price quotations [36,37] to be 15$ per kg. Note that the investment cost (3) does not cover the equipment for reactor cooling. Cost estimates for heat transfer equipment are introduced in Section 2.2.2.

2.1.3. Biological methanation reactor

Continuous biological methanation without biomass digestion is a process under active development. The research focuses on the identification of active anaerobic micro-organisms and the optimization of the gas transfer under relevant process conditions. A wide range of operational process data can be found in the literature, particularly regarding the product gas concentrations. Only a few studies could report an exceptionally high methane concentration of 96% [38,39] in the dry product gas; however, product concentrations from 58% [40] to 85% [12] are commonly reported. The overall process design is strongly dependent on the product methane concentration of the biological unit. Therefore, we consider two optional bioreactor models: A bioreactor reaching 96% CH_4 (BIO1) and one reaching 65% CH_4 (BIO2) in the dry product gas. The product gas leaving the biological methanation reactor is moist. Thus, we calculate the water in the gas stream according to the vapor–liquid equilibrium calculation, shown in Section 2.1.4. Both reactor models operate at ambient pressure and 363.15 K and lose 5% of the reactants to biomass growth. For the CAPEX, we choose an estimate from the literature of EUR 658 K [10], corresponding to $723.8 K. The reference is the smallest fermenter studied by Graf et al. [10] producing 1 MW_{CH_4}, which is slightly larger than the 0.8 MW_{CH_4} needed for converting the aforementioned 2.64 mol_{H_2}/s (AE) to CH_4.

2.1.4. Flash separation

Flash separation is applied to reduce the amount of water in the gas mixture. The process requires cooling, owing to the condensation of the liquid product. The separation result is calculated via vapor–liquid equilibrium at fixed temperature. We describe the separation by the equilibrium relation

$$\begin{aligned} \frac{N_i^l}{\sum_j N_j^l} &= K_i \frac{N_i^{\text{in}} - N_i^l}{\sum_j N_j^{\text{in}} - N_j^l} && \text{for } i \in \widehat{C} \\ K_i - \frac{p_{\text{vp},i}}{p_{\text{in}}} &= 0 && \text{for } i \in \widehat{C} \end{aligned}$$

with $\widehat{C} = \{CO_2, H_2O, CH_4\}$. Phase equilibrium constants K_i are calculated from the pure component vapor pressure $p_{\text{vp},i}$, with the exception of hydrogen, which is assumed to stay in the gas phase owing to its high volatility. We consider a point of operation at

$$\begin{aligned} T^{in} &= 298.15 \text{ K} \\ p^{in} &= 6 \text{ bar}. \end{aligned}$$

The unit material stream output is

$$\begin{aligned} x^{\text{out}}(x, x^{\text{in}}) &= [x^{\text{out},1}(x, x^{\text{in}}), x^{\text{out},2}(x, x^{\text{in}})] \\ x^{\text{out},1}(x, x^{\text{in}}) &= [N_{CO_2}^l, 0, N_{CH_4}^l, N_{H_2O}^l, T^{\text{in}}, p^{\text{in}}] \\ x^{\text{out},2}(x, x^{\text{in}}) &= [N_{CO_2}^{\text{in}} - N_{CO_2}^l, N_{H_2}^{\text{in}}, N_{CH_4}^{\text{in}} - N_{CH_4}^l, N_{H_2O}^{\text{in}} - N_{H_2O}^l, T^{\text{in}}, p^{\text{in}}] \end{aligned}$$

where the liquid phase is considered as waste stream, i.e., it is not considered for recycling. The flash unit requires heat removal to condensate water, but no supply of electrical energy.

$$\begin{aligned} W(x) &= 0 \\ Q(x) &= -\sum_i N_i^l \Delta H_{c,i} \end{aligned}$$

The cost is calculated similarly to the reactor model via

$$\text{CAPEX}(x) = \text{CE}\, C_0 \left(\frac{L}{L_0}\right)^{\alpha} \left(\frac{D}{D_0}\right)^{\beta}$$

with parameters $C_0 = 2,950\$$, $L_0 = 1.22\,\text{m}$, $D_0 = 0.91\,\text{m}$, $\alpha = 0.81$, $\beta = 1.05$ from [35]. Unit parameters L and D were calculated from the liquid flow rate $F^l = \sum_i N_i^l$ via

$\rho = 55345$	Liquid density (mostly water) (mol/m^3)
$\tau = 300$	residence time (rms)
$V = 2F^l\tau/\rho$	vessel volume (m^3)
$D = (V/\pi)^{(1/3)}$	vessel diameter (m)
$L = 4D$	vessel length (m)

in accordance with [35].

2.1.5. Black box separation models

We describe adsorption, absorption, and membrane separation (MEM) processes by simplified black box models. Adsorption, absorption, and membrane separation are technologies commonly applied in practice [15,41]. The variables are the molar flow rates of components.

$$x = [N_{1,CO_2}, N_{1,H_2}, N_{1,CH_4}, N_{1,H_2O}, N_{2,CO_2}, N_{2,H_2}, N_{2,CH_4}, N_{2,H_2O}]$$

We determine the two product streams

$$\begin{aligned} x^{\text{out}}(x, x^{\text{in}}) &= [x^{\text{out},1}(x, x^{\text{in}}), x^{\text{out},2}(x, x^{\text{in}})], \\ x^{\text{out},i}(x, x^{\text{in}}) &= [N_{i,CO_2}, N_{i,H_2}, N_{i,CH_4}, N_{i,H_2O}, T_i, p_i] \quad i = 1, 2 \end{aligned}$$

of a separation unit from a single input stream $x^{\text{in}} = [N_{CO_2}^{\text{in}}, N_{H_2}^{\text{in}}, N_{CO}^{\text{in}}, N_{CH_4}^{\text{in}}, T^{\text{in}}, p^{\text{in}}]$ by predefined parameters T_1, T_2, p_1, p_2 and $s \in [0, 1]^4$ as

$$\left.\begin{aligned} N_{1,j} &= s_j N_{\text{in},j} \\ N_{2,j} &= (1 - s_j) N_{\text{in},j} \end{aligned}\right\} j \in \{CO_2, H_2, CH_4, H_2O\}$$

as well as further energy balances distinct for the specific separation process. The investment costs are calculated from

$$\text{CAPEX}(x) = C_0 \sum_i N_i.$$

Tables 1 and 2 list the values of parameter C_0, which were adapted from the review [15] corresponding to the commercial separation units of the size to treat 500 Nm^3/h, which is closest to the aforementioned a priori gas flow estimate.

We consider Pressure Swing Adsorption (PSA) to separate CO_2 and CH_4. A large variety of established adsorbent materials are suitable for this particular separation task, e.g., zeolites, silica gel, and activated carbon (AC) [42]. Adsorption processes can separate a component to a very high purity. As is well known in the literature [43], CH_4 can be extracted with a purity of more than 99% from CO_2 with zeolites. A

Table 1
Parameters of adsorption black box models.

	PSA (Z)	PSA (AC)	PSA (Z II)	PSA (AC II)
s	[0.01,1,0.85,0]	[0.05,0.99,0.1,0]	[0.15,1,0.99,0]	[0.7,0.99,0.85,0]
p_1(bar)	6	23	6	23
p_2 (bar)	0.2	1.0325	0.2	1.0325
C_0 ($\frac{1e3\$}{mol/s}$)	475.4	475.4	950.7	950.7

$T_1 = T_2 = 298.15$ K.

Table 2
Parameters of adsorption, absorption and membrane separation black box models.

	TSA	ASC	WSC	MEM
s	[0.95,1,0.99,0]	[0.95,1,0.99,0]	[0.95,1,0.99,0]	[0.95,1,0.99,0]
T_1 (K)	298.15	333.15	298.15	298.15
p_1 (bar)	6	1.0325	6	6
T_2 (K)	418.15	413.15	–	298.15
p_2 (bar)	6	1.5	–	0.2
C_0 ($\frac{1e3\$}{mol/s}$)	475.4	907.5	172.9	570.4

drawback of this method, however, is that large quantities of methane remain in the off-gas. In alignment with studies on the adsorbent zeolite 5A [43] we chose parameters denoted PSA (Z) in Table 1. We constrain the inlet pressure to the adsorption pressure $p^{in} \geq p_1$, making no additional compression at this unit necessary. Decompression of the column is performed via a subsequent state changer model, see Section 2.1.6. Furthermore, we assume that no work can be recuperated from the depressurization state to the desorption pressure p_2 and that the temperature oscillations during adsorption and desorption result in negligible heat flows. Thus

$$W(x) = 0$$
$$Q(x) = 0.$$

In a similar manner, we consider the separation of hydrogen via the adsorbent AC [44]. Table 1 gives the parameters in the column labeled PSA (AC). This technology can be applied after methanation to recycle super-stoichiometric amounts of H_2.

To avoid damage to the adsorbent, the gas stream entering the PSA unit must be dry; therefore, we add the constraint

$$N^{in}_{H_2O} = 0$$

to the model.

To separate both CO_2 and CH_4 with a very high purity, two PSA units are used in parallel [43]. The setup is depicted and described in Fig. 3. The unit in position (P1) in Fig. 3 has the operating parameters given by PSA (Z) or PSA (AC) in Table 1. The unit in position (P2) has the parameters given in Table 1 by PSA (Z II) or PSA (AC II), respectively. We calculate the additional work for the repressurization via the state changer model (see Section 2.1.6). We consider the two-PSA setup as a single-unit alternative to the one-PSA model in the superstructure.

We apply Temperature Swing Adsorption (TSA) to dry the gas

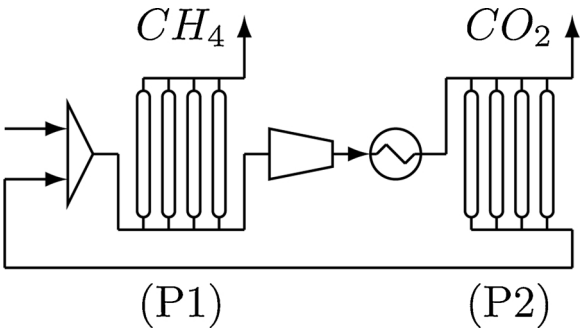

Fig. 3. Two connected PSA units for CO_2/CH_4 separation. A typical PSA unit for separation of binary mixtures produces only one product gas stream at a very high purity. In this application, the unit (P1) produces high-purity CH_4 and a mixture of CH_4 and CO_2. We achieve high product gas concentrations for both product streams by redirecting the second gas stream to another PSA unit (P2). This unit extracts CO_2 at a high concentrations and redirects the second stream, again a mixture, back to the first unit. To implement the cyclic depressurization and repressurization of the PSA unit, we add an additional compressor between the units.

mixture with parameters shown in Table 2. Furthermore, heat is required for the desorption of the adsorbent.

$$Q(x) = \sum_i N_{2,i} c_{p_i} (T_2 - T_1)$$

An alternative process to separate CO_2 from CH_4 is absorption. Both water and amine scrubbing are widely applied in the industry [41,45]. In alignment, we include the separation via chemical scrubbing with amines (ASC) and that with water scrubbing (WSC) in the analysis with parameters shown in Table 2. Note, that WSC is modeled to have a single output material stream containing mostly methane, because the off-gas is a mixture of carbon dioxide, oxygen, and nitrogen not suitable for further utilization in the process. For ASC, work and heat demands are calculated via

$$W(x) = w_{ASC} \sum_i N^{in}_i$$
$$Q(x) = q_{ASC} \sum_i N^{in}_i,$$

where $w_{ASC} = 13.8$ and $q_{ASC} = 54.1$. The parameters for MEM were taken from [41,45]. As for PSA, drying of the gas stream is performed prior to application of this unit.

2.1.6. State changer

To model the temperature and pressure changes of a material stream between unit operations, we include state changers. We model the isothermal compression ($T^{out} \geq T^{in}$) to calculate the reversible work demand with

$$W^{rev}(x) = \sum_i N_i R T^{in} \log\left(\frac{p}{p^{in}}\right). \tag{4}$$

Assuming a working efficiency of 80%, we get $W(x) = W^{rev}(x)/0.8$ and an additional heat stream

$$Q^1(x) = -W(x). \tag{5}$$

Furthermore, a temperature change is calculated according to

$$Q^2(x) = \sum_i N_i c_{p_i} (T^{in})(T^{out} - T^{in}) \tag{6}$$

The capital cost of a compressor is calculated via

$$C = \mathrm{MFCE}\, C_0 \left(\frac{W}{S_0}\right)^{\alpha} \tag{7}$$

with $C_0 = 23000\$$, $S_0 = 74.6$ kW, $\alpha = 0.77$, MF = 3.61.

2.2. Superstructure model

To describe the setup of a superstructure, we use a directed, acyclic graph $\mathcal{G} = (\mathcal{V}, \mathcal{E})$, where nodes $\mathcal{V}$ denote the unit models and edges $\mathcal{E}$ represent the intermediate material streams. We define $p: \mathcal{V} \to P(\mathcal{V})$, $p(U) = \{V \in \mathcal{V}: (V, U) \in \mathcal{E}\}$ where $P(\mathcal{V})$ denotes the power set of $\mathcal{V}$. With this mapping, we can derive constraints restricting solutions to a single path through the connection graph.

$$x_{T,U} \leq \sum_{V \in p(U)} x_{T,V} \leq 1 \quad \forall\, U \in \mathcal{V} \tag{8}$$

$$x_{T,V} \leq \sum_{U \in \hat{p}(V)} x_{T,U} \leq 1 \quad \forall\, V \in \mathcal{V} \tag{9}$$

where $x_{T,U} \in \{0, 1\}$ denotes an indicator variable assigned to node $U \in \mathcal{V}$ and $\hat{p}(U) := \{V \in \mathcal{V} | V \in p(U)\}$ (Fig. 4).

Indicator variables indicate whether the respective node U is active ($x_{T,U} = 1$) or inactive ($x_{T,U} = 0$), given a solution to the superstructure problem. The constraints of active nodes must hold, whereas for inactive nodes, they are deactivated. Constraints corresponding to a unit operation model U can be deactivated via different formulations. A

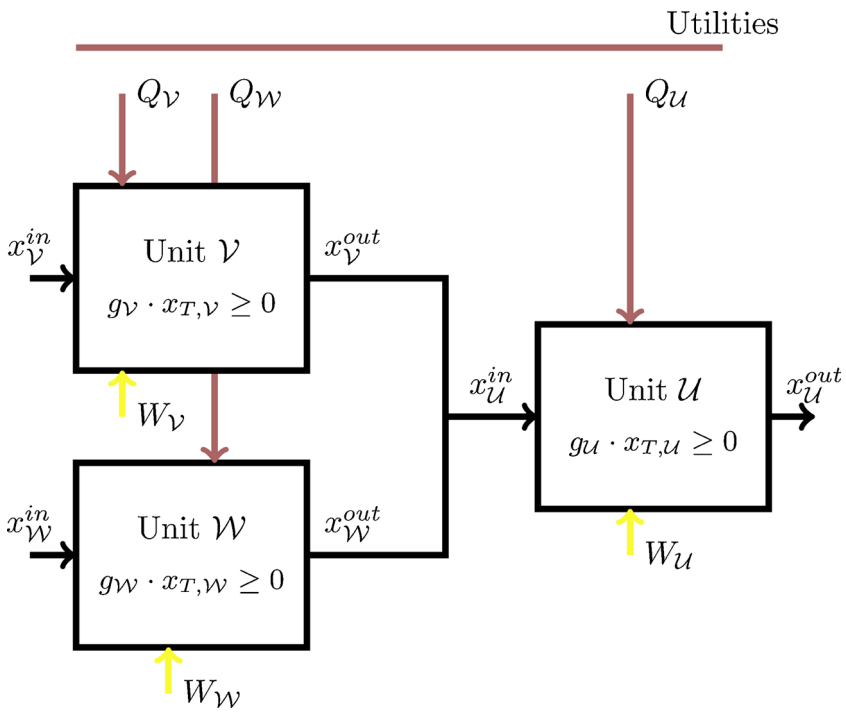

Fig. 4. Scheme of connected unit level models to a structure with connections $p(u) = \{V, W\}$. We route material streams of parent nodes V and W to a child node U. The corresponding indicator variables $x_{T,U}$, $x_{T,V}$, $x_{T,W}$ determine whether a unit is part of a solution candidate. We obtain the work demand of the process by summing up the work demand of the individual nodes. We collect the heat flows and consider them for indirect heat integration.

classic example is the big M formulation, where M is chosen large enough such that a constraint $g_U(x_U, x_U^{\text{in}}) \leq 0$ is not enforced if $x_{T,U} = 0$,

$$g_U(x_U, x_U^{\text{in}}) \leq M(1 - x_{T,U}).$$

This particular formulation has the advantage of being linear if g_U is linear. However, weak relaxations make this formulation unsuitable for practical applications if the upper bound on the constraints is unknown or very large. Therefore, we apply this formulation only to the box constraints and to calculate the material stream x_U^{in} entering unit U from the output streams $x_{p(U)}^{\text{out}} := \{x_V^{\text{out}} : V \in p(U)\}$ of connected units, where a suitable upper bound is known a priori. The box constraints are used to fix variables of inactive models. A variable is forced to zero via (10) or to the lower bound via (11) if zero is not part of its domain.

$$x_{T,U}\,\text{lb}_U \leq x_U \leq x_{T,U}\,\text{ub}_U \quad \text{if } 0 \in [\text{lb}_U, \text{ub}_U],\ U \in \mathcal{V} \tag{10}$$

$$\text{lb}_U \leq x_U \leq \text{lb}_U + x_{T,U}(\text{ub}_U - \text{lb}_U) \quad \text{if } 0 \notin [\text{lb}_U, \text{ub}_U],\ U \in \mathcal{V} \tag{11}$$

For nonlinear inequalities, we chose a complementary formulation (12) to achieve the same result.

$$x_{T,U}\,g_U(x_U, x_U^{\text{in}}) \leq 0 \quad U \in \mathcal{V} \tag{12}$$

For linear equations, SCIP supports indicator formulations within the framework. We apply this method to implement the remaining linear equations.

2.2.1. Recycle

The superstructure includes recycling from separation units back to the reactor. For a recycle stream l, variable $\eta \in [0, 0.95]$ describes the fraction of the product stream recycled back to the process. The remainder is purged, i.e., considered a waste stream. PSA, ASC and MEM are considered for recycle. For processes with a recycle loop, we add the costs of an additional mixer to the CAPEX.

2.2.2. Heat integration

Heat integration between the unit models and utilities covers the heat and cooling demands of the process units. In addition, heat sinks and sources throughout the process are identified to detect the internal utilization potential of the heat flows. To implement this, heat flows must entail information regarding the temperature, as heat can only be supplied from sources of higher temperature.

Heat integration is performed indirectly, according the method proposed by Schack et al. [46] and Liesche et al. [47]. For this purpose, we assume that we have utilities at temperatures $\widehat{T}_i$, $i \in \{1, \ldots, n_U\}$, where $n_U \in \mathbb{N}$ denotes the number of utilities. A minimal temperature difference of $\Delta T = 10\,\text{K}$ must hold for the heat integration between a utility and a unit for realistic heat transfer rates. As opposed to the model introduced by Schack et al. [46], we consider the unit temperatures to be variables; therefore, we do not classify the heat flows into the three cases (full, partial, or no heat integration) a priori. Instead, we differentiate between two types of heat flows: Heat flow with a temperature change between two temperatures T_{in}, T_{out} (type I) and heat flow at a constant temperature (type II), e.g., excess heat from the isothermal reactor model. For heat flows of type I, we calculate the heat flow $Q_{j,i}$ between utility $i \in \{1, \ldots, n_U\}$ and unit $j \in \{1, \ldots, n\}$ with $Q_j = C_{p_j}(T_{j,\text{out}} - T_{j,\text{in}})$ via the constraints

$$\underline{c}_{j,I} C_{p_j} \leq \sum_{i \in I} Q_{j,i} \leq \bar{c}_{j,I} C_{p_j} \tag{13}$$

with

$$\bar{c}_{j,I} = \max\{\min_{i \in I}\{T_{j,\text{out}}, \widehat{T}_i - \Delta T\} - T_{j,\text{in}}, 0\} \tag{14}$$

$$\underline{c}_{j,I} = \min\{\max_{i \in I}\{T_{j,\text{out}}, \widehat{T}_i + \Delta T\} - T_{j,\text{in}}, 0\} \tag{15}$$

for all $I \subset \{1, \ldots, n_U\}$. If the direction of the heat flow is known a priori (e.g., heating of the TSA desorption gas), some of the minimum and maximum functions can be omitted.

In addition, for heat flows of type II, the constraints

$$\min\{Q_j, 0\} \leq \sum_{i \in I} Q_{j,i} \leq \max\{Q_j, 0\} \tag{16}$$

$$\min\{\sum_{i \in I} Q_{j,i}, 0\}(\min_{i \in I} \widehat{T}_i - \Delta T - T_j) \geq 0 \tag{17}$$

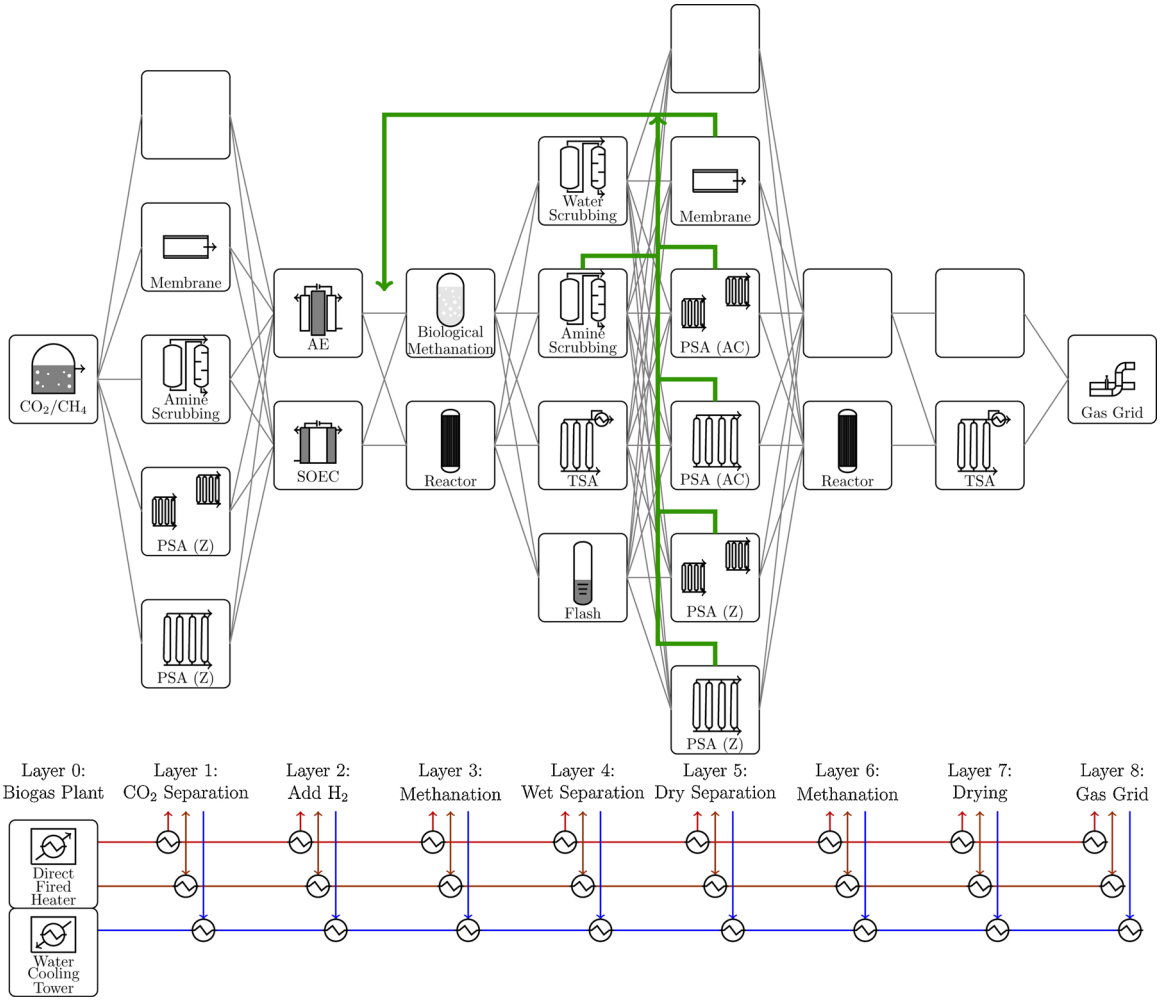

Fig. 5. Graph of the superstructure. The superstructure graph has 7 layers between the biogas plant and gas grid. Recycling is considered from layers 4 and 5 to the reactor at layer 3. Layers 1, 5, 6, and 7 may be skipped by the solution, which is indicated in the figure by the empty boxes. We have different technologies for the purification of CO_2 in layer 1. Layer 2 includes the choice of electrolyzer, and layer 3 provides the choice of the first methanation step. After methanation, the gas mixture includes water as a side product. Therefore, we consider separation technologies which are not damaged by water in layer 4. These separation technologies in layer 4 can separate either reactants or water from the gas mixture. In layer 5, reactants can be separated from a dry gas mixture and recycled back to the reactor. Finally, a second reactor can be added in layer 6, which makes a final drying effort in layer 7 necessary. Each unit has the option to take or supply heat to the utilities. Sulfur components in the gas mixture after biological methanation cause catalyst deactivation in a downstream catalytic reactor. Thus, we restrict the solution from choosing the methanation reactor in layer 6, if biological methanation was chosen in layer 3.

Table 3
Objective values.

Electrolyzer		AE		SOEC	
H_2 constraint		Eq. (23)	Eq. (24)	Eq. (23)	Eq. (24)
η (%)	(O1)	50.0	50.8	65.1	65.8
CAPEX ($)		3,273,748	2,811,082	5,645,154	5,203,597
η (%)	(O2)	45.3	45.3	58.6	65.0
CAPEX ($)		2,537,820	2,537,820	4,990,043	5,276,057
η (%)	(O3)	45.7	45.8	64.5	61.4
CAPEX ($)		2,474,590	2,478,606	6,365,894	5,474,382

Values of the efficiency and CAPEX for the 12 considered cases after global optimization. The results with respect to objectives (O1) and (O2) give different values on the Pareto front of efficiency and CAPEX. Meanwhile, objective (O3) corresponds to the TAC.

$$\max\{\sum_{i\in I} Q_{j,i},\, 0\}(\max_{i\in I} \widehat{T}_i + \Delta T - T_j) \geq 0 \tag{18}$$

can be simplified significantly, if the flow direction is known a priori. This is the case for all heat flows of type II in the current application.

The external heat demand/surplus of a utility i is denoted by

$$Q_{\text{ext},i} = \sum_{j\in\{1,\ldots,n\}} Q_{j,i}. \tag{19}$$

To cover the external heat demand of utilities, we add directly fired heaters. Cooling is performed via water cooling towers. We calculate the capital costs of heat exchangers and directly fired heaters via the Guthrie equation (7). For heat exchangers, the parameters $C_0 = 5,000$\$, $S_0 = 37.2\,\text{m}^2$, $\alpha = 0.65$, MF = 3.3 and for directly fired heaters $C_0 = 20,000$\$, $S_0 = 1465\,\text{m}^2$, $\alpha = 0.77$, MF = 2.73 were taken from Biegler et al. [35]. The cooling of utilities is performed via a cooling tower. The capital cost of a cooling tower was calculated by EWK [48], specifically to meet the cooling demand of the coldest utility ($T = 289.15$ K). The cost including frost protection but without transport is 38,477 €. Assuming a rate of exchange of 1.1, this corresponds to 42,305\$.

Note that the hottest and coldest utility temperatures are fixed by the process temperature boundaries, i.e., $T_1 = T_{\min} - \Delta T$, $T_{n_U} = T_{\max} + \Delta T$. This is necessary to make heat transfer realistic and the integration feasible. Temperatures of additional utilities $T_i \in [T_{\min}, T_{\max}]$, $i \in \{2, \ldots, n_U\}$ if $n_U > 2$ are optimized by the solver.

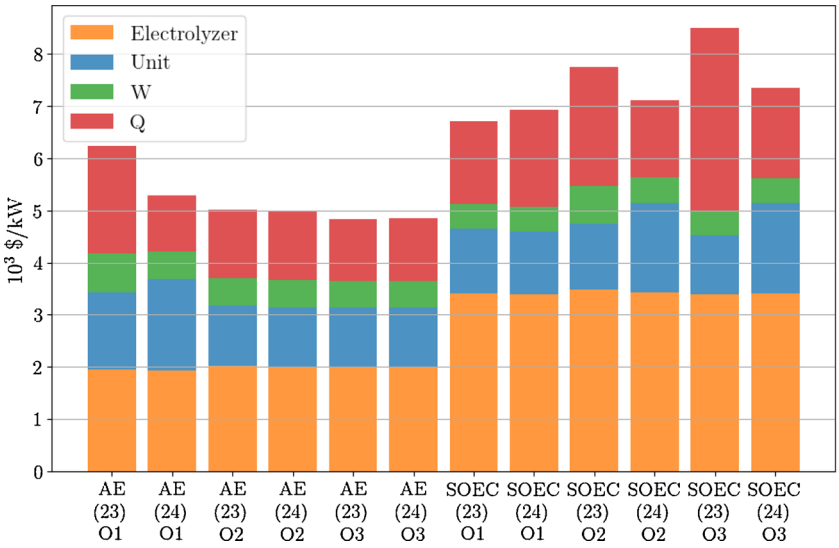

Fig. 6. CAPEX values of the optimization results. The figure shows the contributions of the unit, compressor (W), and heat exchanger (Q) costs to the CAPEX. The CAPEX is scaled to the plants product capacity of total CH_4 in terms of LHV in kW. Note that SOEC is a technology on demonstration level and has potential for cost improvement. The concentration of H_2 is limited by Eq. (23) or (24) corresponding to 2 mol% and 10 mol% H_2 respectively.

Table 4
Contribution of product, heat, and work to the exergetic efficiency η.

Case			η (%)	LHV_{CH_4} (kW)	F_{CH_4} (kW)	F_W (kW)	F_Q (kW)
AE	(23)	(O1)	50.0	525.0	544.1	40.8	2.8
AE	(24)	(O1)	50.8	530.8	550.3	41.4	1.5
AE	(23)	(O2)	45.3	505.6	522.3	33.2	36.1
AE	(24)	(O2)	45.3	510.7	528.3	39.2	36.1
AE	(23)	(O3)	45.7	511.2	529.1	39.3	32.8
AE	(24)	(O3)	45.8	511.7	529.0	39.3	31.7
SOEC	(23)	(O1)	65.1	744.2	771.3	54.6	65.2
SOEC	(24)	(O1)	65.8	750.9	778.2	55.2	65.2
SOEC	(23)	(O2)	58.6	728.6	755.1	75.3	93.4
SOEC	(24)	(O2)	65.0	742.0	769.0	54.8	64.6
SOEC	(23)	(O3)	64.5	748.3	775.5	54.8	75.8
SOEC	(24)	(O3)	61.4	745.1	772.2	55.1	103.0

The exergy values of F_{CH_4}, F_W, and F_Q at the optimal solution determine the efficiency η via Eq. (20). In addition the lower heating value of the product stream (LHV_{CH_4}) is shown. Note, that this value includes the contribution of hydrogen in the product gas.

Increasing the number of heat exchangers is expected to increase the heat network cost and, therefore, the capital cost of the plant. In the case of two utilities, no indirect heat integration can be performed. All heat is flowing from the hot utility to the process and from the process to the cold utility. Therefore, we chose $n_U = 3$.

2.2.3. Objective

We optimize the superstructure with regards to two objectives: to maximize the exergetic efficiency, which is a goal of many climate change mitigation actions both nationally and internationally, and to minimize investment costs, which is relevant for plant operators. Furthermore, the two objectives are combined via linear combination to get Pareto optimal solutions to the multi-objective optimization problem.

We describe efficiency via chemical exergy of the produced methane and the investment cost via total process CAPEX. The efficiency η is calculated in reference to the 1 MW used for water electrolysis as

$$\begin{aligned}\eta &= \frac{F_{CH_4} - F_W - F_Q}{F_{ref}} \\ &= \frac{\sum_{j\in\{1,\dots,n_P\}} F^j_{CH_4} - F^{feed}_{CH_4} - \sum_{u\in\mathcal{V}} W_U}{1000} \\ &\quad \frac{- \sum_{i\in\{1,\dots,n_U\}} (1 - \frac{T_0}{T_i}) \max\{0, Q_{ext,i}\}}{1000}\end{aligned} \tag{20}$$

where $F^j_{CH_4}$ denotes the chemical exergy of material stream j leaving or entering the process. The heat demand of the utilities is weighted by the term $(1 - \frac{T_0}{T_i})$, which is the efficiency of a Carnot engine. The fraction $\frac{T_0}{T_i}$

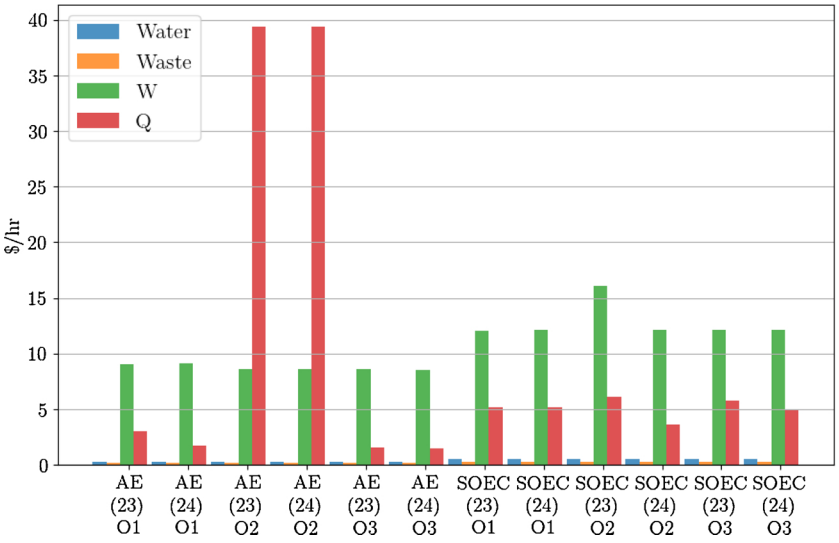

Fig. 7. OPEX, operating costs of the optimization results. The figure shows the contribution of water, waste water, work (W) and heat (Q) to the OPEX. We do not include 220 $/h for 1 MW of electrical energy for water electrolysis. Water and waste water are small in comparison to the costs from work and heat. In particular, if indirect heat integration is avoided to reduce CAPEX (O2) the heat exchange causes significant increase of the OPEX. The concentration of H_2 is limited by Eq. (23) or (24) corresponding to 2 mol% and 10 mol% H_2, respectively.

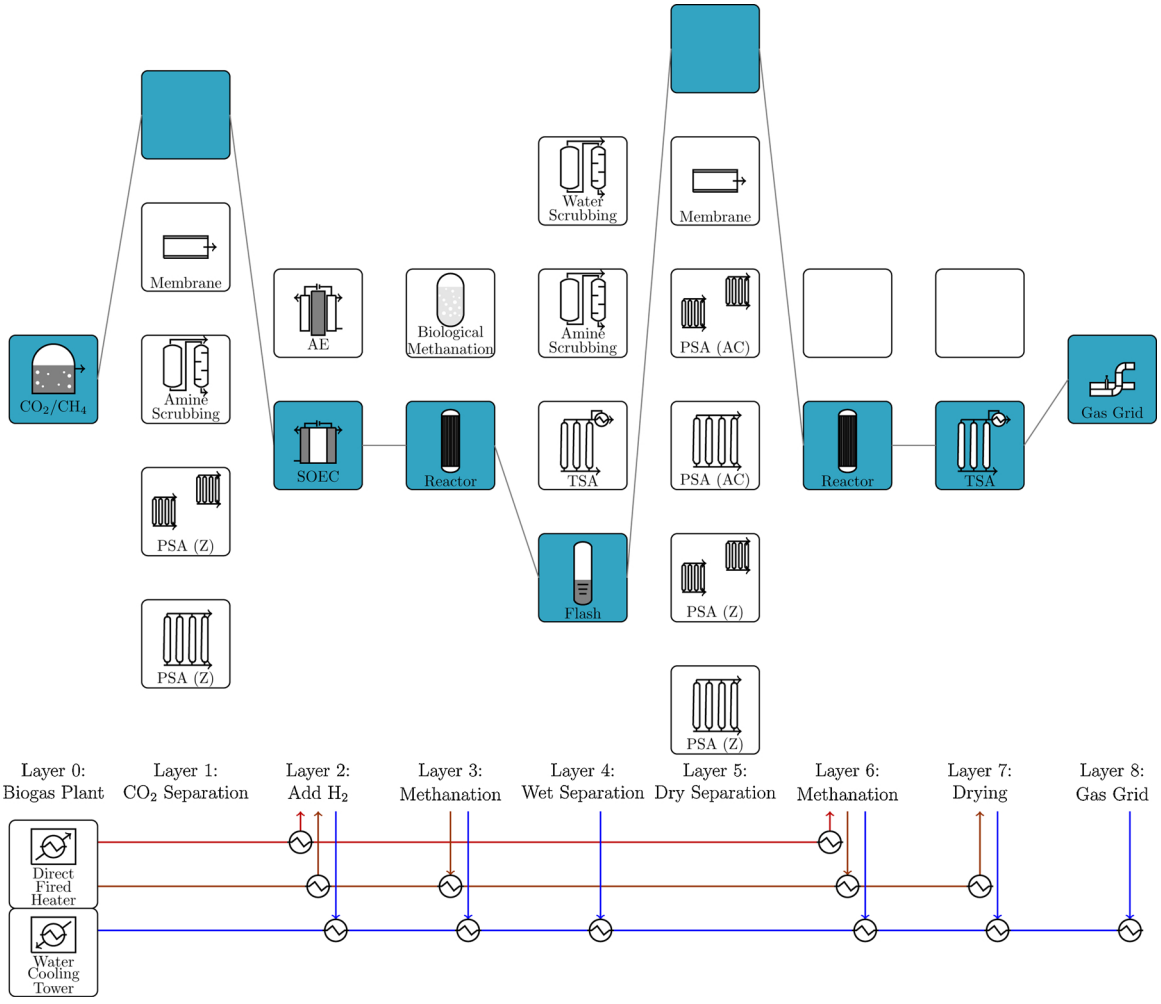

Fig. 8. Solution path: Two reactor configuration. The configuration is optimal in terms of efficiency and CAPEX for the choice of SOEC electrolyzer. If we replace SOEC by AE in layer 3, the same path through the rest of the superstructure is chosen, with changes to the heat exchanger network.

relates the temperature of the utility i to the ambient temperature $T_0 = 298.15$ K. Electrical energy directly relates to its exergetic value.

A material stream leaving the superstructure is evaluated via the chemical exergy of methane $e_{CH_4} = 831.2$ kJ/mol and hydrogen $e_{H_2} = 236.1$ kJ/mol if the requirements for feed into the gas grid, see Eqs. (23)–(25), are met. If the requirements are not met, the respective product stream has no contribution to the objective.

The process CAPEX acts as a penalty term. The most efficient solutions tend to include extensive heat exchanger networks to integrate even very small heat flows back into the process. This leads to very costly processes. By adding the penalty term to the objective, these solutions to the superstructure are avoided. The objective is given by

$$f_1(x) = w_C C - w_\eta \eta \tag{21}$$

where the weights w_C and w_η determine the position of the solution along the Pareto front.

The process CAPEX is the sum of the unit model CAPEX contributions:

$$C = \sum_{u \in \mathcal{V}} \text{CAPEX}_U(x_U)$$

Alternatively to multi-objective optimization, we consider the total annual costs (TAC) as an objective for optimization. The TAC are calculated from the CAPEX and the operating costs (OPEX) as

$$\text{TAC} = \text{OPEX} + \left(\frac{z}{1-(z+1)^{-t_{\text{payback}}}}\right)\text{CAPEX} \tag{22}$$

with an interest rate $z = 0.06$ and a payback time $t_{\text{payback}} = 20$ a. For the calculation of the OPEX, we assume prices of 20 ct/kWh for electrical energy, 1.89$/kg water, 2.64$/kg waste water removal, and 2.3 ct/kWh steam.

2.2.4. Composite model

A superstructure, including a methanation reactor, AE, SOEC, PSA (zeolite), PSA (AC), double PSA, TSA, flash condensation, ASC, WSC, MEM, compression, heating/cooling, a mixer, recycling and indirect heat integration was built. The overall superstructure optimization problem is given by

$$\begin{aligned} \min_{x=[x_T, x_\mathcal{V}, E_{CH_4}, W_\dot{Q}, E_\dot{Q}]} \quad & f(x) \\ \text{s. t.} \quad & (8)-(19) \\ & x_U \in \mathbb{R}^{n_U} \qquad \forall\, U \in \mathcal{V} \\ & x_T \in \{0,1\}^n. \end{aligned}$$

where $x_\mathcal{V} = \{x_U : U \in \mathcal{V}\}$ and $f(x)$ relates to either the linear combination of efficiency and CAPEX (21) or the TAC (22). The structure is shown in Fig. 5, with a total of 600 alternative process routes.

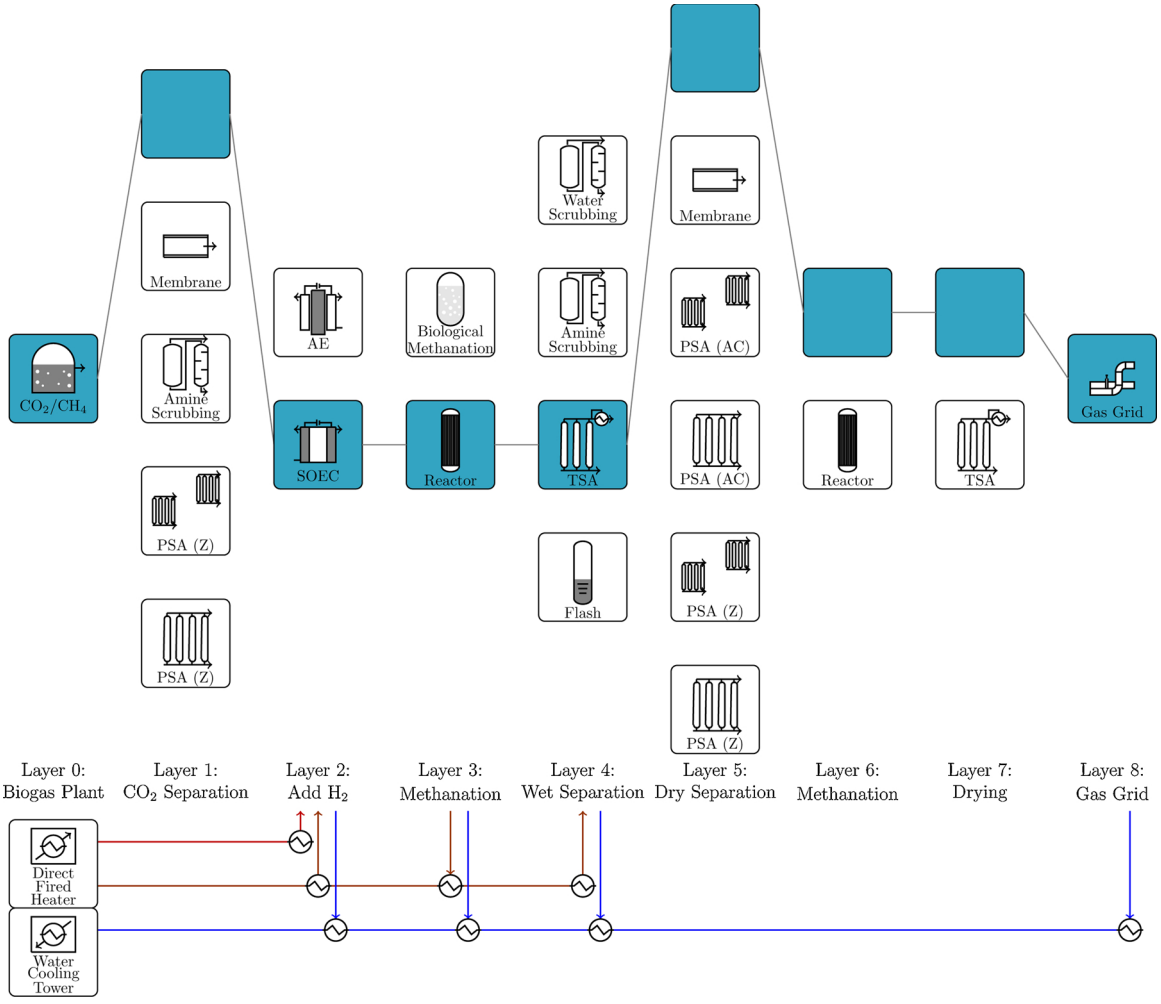

Fig. 9. Solution path: single reactor configuration. The configuration is optimal in terms of efficiency for the choice of SOEC electrolyzer if a large quantity of hydrogen can be supplied to the natural gas grid. If we replace SOEC by AE in layer 3, the same path through the rest of the superstructure is chosen, with changes to the heat exchanger network.

Table 5
Results of the optimization with biological methanation.

Electrolyzer		AE		SOEC	
Bioreactor		BIO1	BIO2	BIO1	BIO2
η (%)	(O1)	47.0	46.5	56.1	55.3
CAPEX ($)		3,517,540	3,839,147	5,709,424	6,134,440

The table shows the results of the optimization with biological methanation with respect to (O1). We consider the two bioreactors BIO1 and BIO2 with 96% and 65% of CH_4 in the dry product gas, respectively. Optimization with respect to (O2) or (O3) shows almost identical results to the result of (O1). This is due to the limitation of the heat integration for this case.

3. Results

3.1. Catalytic methanation

We solve the superstructure model introduced in the previous section under various conditions.

- **Electrolyzer technology (AE or SOEC)**
  AE are well-established technologies, commercially available at various scales. Because of this, they have lower cost than other water electrolysis technologies. However, AE have comparably low efficiency. SOEC operate at high temperatures, significantly increasing cell efficiency. The technology is in its early stage and, therefore, still quite expensive. Instead of allowing the solver to choose between these two technologies, we manually choose one of the technologies. This allows us to directly observe the influence of the choice of electrolyzer on the optimization result.
- **Weight of linear combinations of the objectives**
  To compare the different alternative solutions, we select different points of the Pareto front via linear scaling of the objectives. We consider the weights $w_\eta = 1$, $w_C = 10^{-8}$ to focus on the process efficiency (O1). This typically leads to very extensive heat integration networks that utilize heat flows within the process. This is expected to lead to high capital costs. Therefore, we consider $w_\eta = 1$, $w_C = 10^{-5}$ as an alternative (O2). These weights scale efficiency and capital costs to roughly the same order of magnitude. Thus, we can obtain an efficient process with reasonable capital costs. We do not optimize with regard to only capital costs, as this typically leads to solutions close to an efficiency of 0%. Alternatively, we optimize the system with respect to the TAC (O3).
- **Constraints for feed into the gas grid**
  We consider two different thresholds for the amount of hydrogen allowed in the gas grid. Currently restrictive constraints of 2 mol% H_2 need to be fulfilled in some areas. However, to facilitate the implementation of power-to-gas technologies in the future, these constraints are under discussion. Local distributors already allow for the feed-in of gas with up to 10 mol% H_2. We consider the less

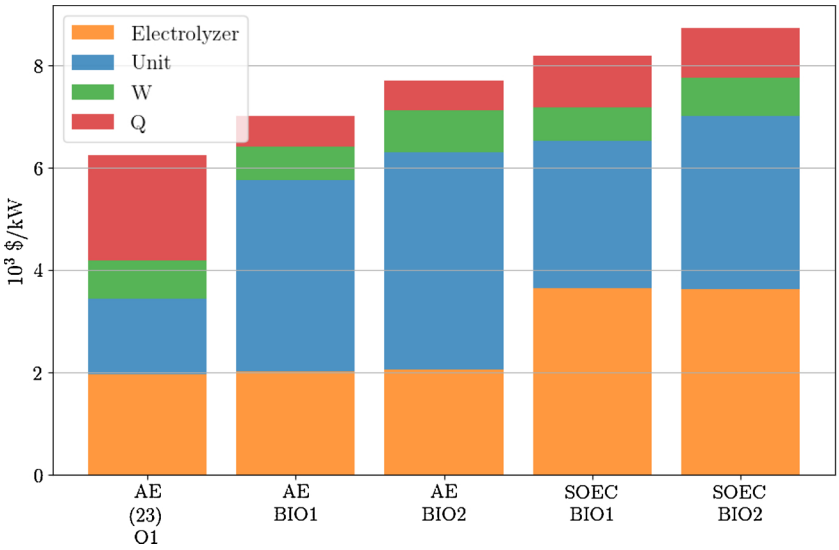

Fig. 10. CAPEX values of the optimization results for biological methanation. The figure shows the contributions of the unit, compressor (W), and heat exchanger (Q) costs to the CAPEX. The CAPEX is scaled to the plants product capacity of total CH_4 in terms of LHV in kW. For reference, the value AE (23) O1 for catalytic methanation is shown, which is also included in Fig. 6.

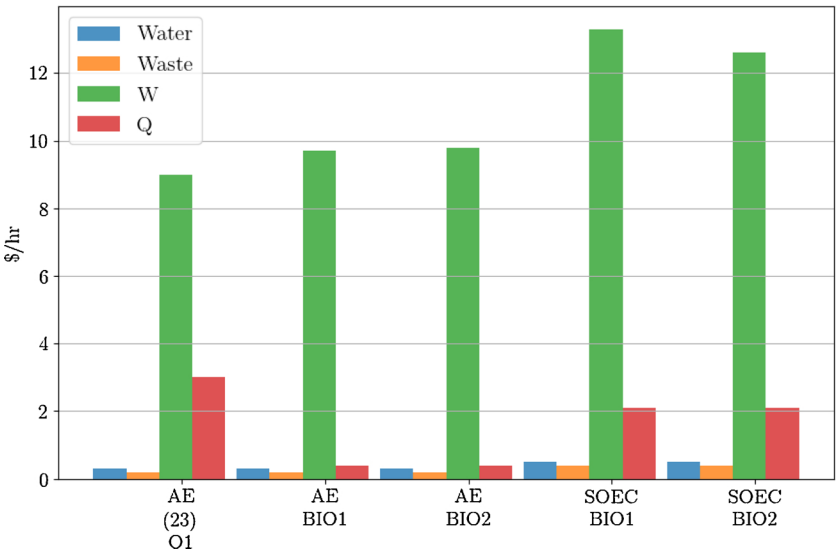

Fig. 11. OPEX, operating costs of the optimization results. The figure shows the contribution of water, waste water, work (W) and heat (Q) to the OPEX. We do not include 220 $/h for 1 MW of electrical energy for water electrolysis. For reference, we show the value AE (23) O1 for catalytic methanation, which is also included in Fig. 6.

restrictive bound of 10 mol% H_2 as an alternative to the 2 mol% H_2 constraint. The constraints for the two cases are given by (23) and (24), where x_i and C_i denote the molar fraction and concentration of component i.

$$\left.\begin{aligned} x_{H_2} &\leq 0.02 \\ 0.95 &\leq x_{CH_4} \end{aligned}\right\} \tag{23}$$

$$\left.\begin{aligned} x_{H_2} &\leq 0.1 \\ 0.90 &\leq x_{CH_4} \end{aligned}\right\} \tag{24}$$

In both cases

$$\left.\begin{aligned} x_{CO_2} &\leq 0.05 \\ C_{H_2O} &\leq 200\,\text{mg/m}^3 \\ p &= 16\,\text{bar} \\ T &= 298.15\,\text{K} \end{aligned}\right\} \tag{25}$$

must hold in addition.

We perform global optimization for the 12 different introduced cases. After fixing the choice of electrolyzer, we have a total of 3175 variables of which 33 are binary. The values of the objective functions after optimization are shown in Table 3. Fig. 6 shows a comparison of the CAPEX values of the different cases. More detailed capital investment costs of the solutions can be found in the Supplementary Material (Table 4).

Two different process routes were chosen by the solver. A cascade of two reactors with intermediate water extraction was used, if only 2 mol % of hydrogen can be supplied to the gas grid, according to the constraints (23). The configuration is shown in Fig. 8. If a higher concentration of hydrogen can be supplied to the grid (24), a second reactor for methanation is not needed. In this case, focusing on the efficiency results in the process configuration, shown in Fig. 9. The cases for which this configuration was optimal are marked blue in Table 3. This configuration results in reduced capital investment costs. Simultaneously, the efficiency of the processes is increased. This effect occurs because less hydrogen is converted to methane. This reduces the exergetic losses in the chemical conversion steps.

If the weights of the objective favor the efficiency objective (O1), the optimal intermediate utility temperature is 570 K. This temperature is directly below the optimal reactor temperature with a difference equal to $\Delta T = 10$ K. This allows the maximal supply of excess heat of the reactor to this utility. The excess heat is then used to heat other process elements. If the CAPEX is weighted higher (O2), internal heat integration is omitted. Instead all heat is supplied and withdrawn externally. This reduces the costs of the heat integration network significantly, as the detailed costs in the Supplementary Material show.

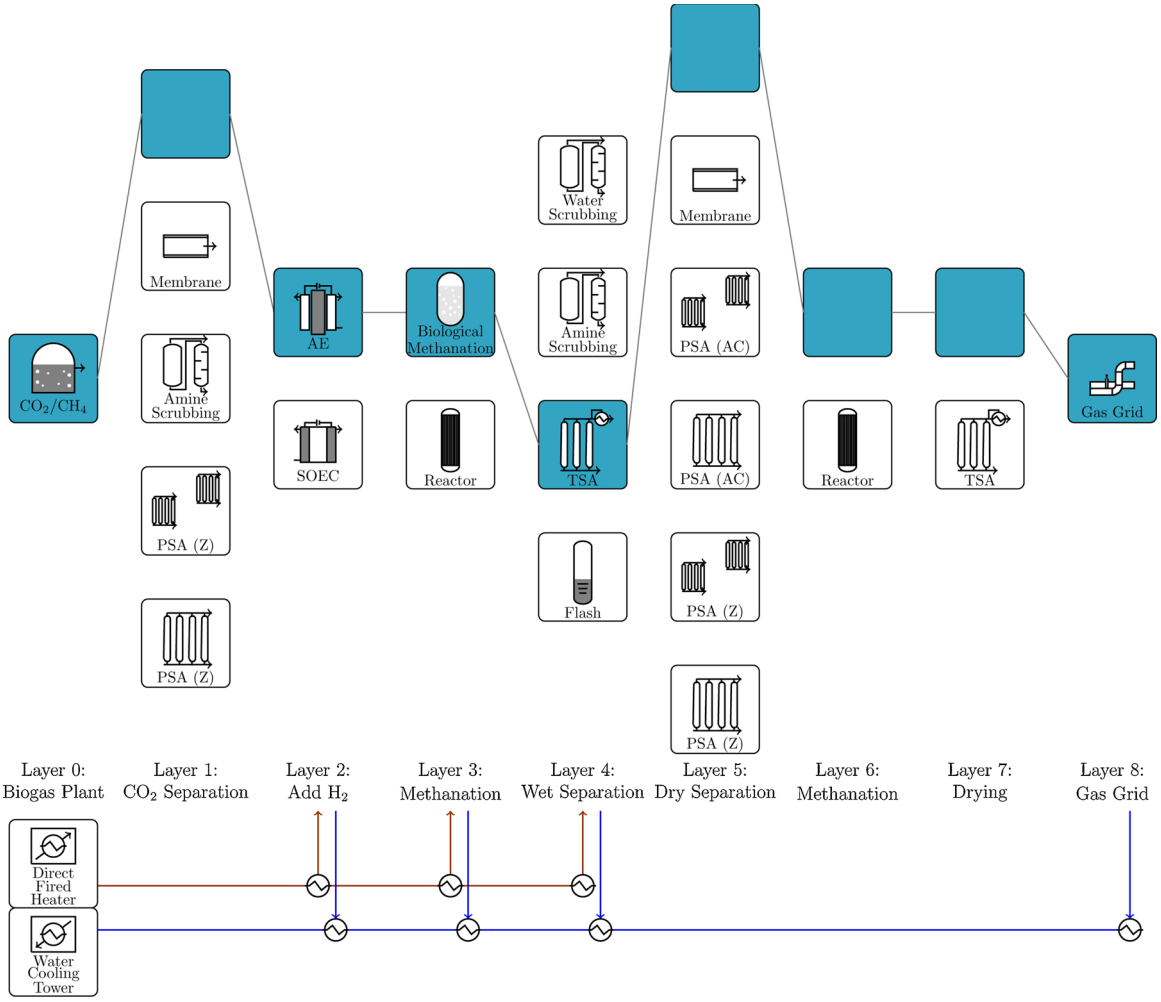

Fig. 12. Solution path: biomethanation with high CH_4 product concentration. The configuration is optimal in terms of efficiency for the choice of AE if a high concentration of methane can be produced by the bioreactor.

For example in the case of AE and grid constraints (23), the costs for the heat exchanger network are reduced from 2063\$/kW_{CH_4} to 1263\$/kW_{CH_4} by avoiding internal heat integration, where kW_{CH_4} denotes the energy of the product gas calculated by the lower heating value. Results of optimization of the superstructure with respect to TAC (O3) give very similar results. The results show adaptation of the extent of the heat exchanger network to the objective.

By using SOEC for water electrolysis, a higher process efficiency can be reached. This comes with a great increase in capital costs, roughly double than for using AE for water electrolysis. Furthermore, the results show that if heat integration is avoided to reduce capital costs, supplying heat to the system greatly reduces the system efficiency.

For the solutions of (O1) and (O2), we estimate the OPEX after optimization. The results are shown Fig. 7, together with the product value. The cost of electrical energy, denoted as W, does not include electricity for water electrolysis, which adds up to an additional cost contribution of 220\$.

The shortcut models used are afflicted with inaccuracies, which propagate to the optimal solution. Other solutions to the superstructure problem have objective values close to the global optimum, such that a clear optimal process must be determined with more accurate models. We consider a few other configurations to compare with the global optimal solution.

For the case of AE and grid specification (23), another interesting configuration includes the separation of the CH_4/CO_2 gas mixture prior to the methanation reactor. Utilization of membrane separation for this task gives an efficiency of 49.4% for (O1), compared with the 50.0% of the optimal solution. Furthermore, the unit costs increase from \$1.804M to \$1.817M, which is negligible with the given accuracy of the models.

Alternatively, we calculate the objective value of replacing the second methanation reactor by the separation and recycling of reactants. This process configuration has promising efficiency at higher process pressures of 13 bar [49]. For the current study, at lower process pressure of 6 bar, the configuration has an efficiency of 47.9%. We attribute the decrease in efficiency to the shortcut model for gas separation. For the gas separation, Uebbing et al. [49] used a more detailed PSA model, which resulted in better separation properties.

3.2. Biological methanation

None of the previous process design solutions included the biological methanation in layer 3. To compare the biological methanation process with the previous results, we enforce the biological methanation to be chosen by the solver by fixing the corresponding indicator variable to be 1. The results of the optimization, including AE and SOEC, are shown in Table 5. In the previous section, the methanation reactor was found to act as a significant heat source. The bioreactor, however, operates at lower temperatures, strongly limiting the heat integration within the process. This contributes to the decrease in the overall process efficiency shown in Table 5, as compared with that of the previous section.

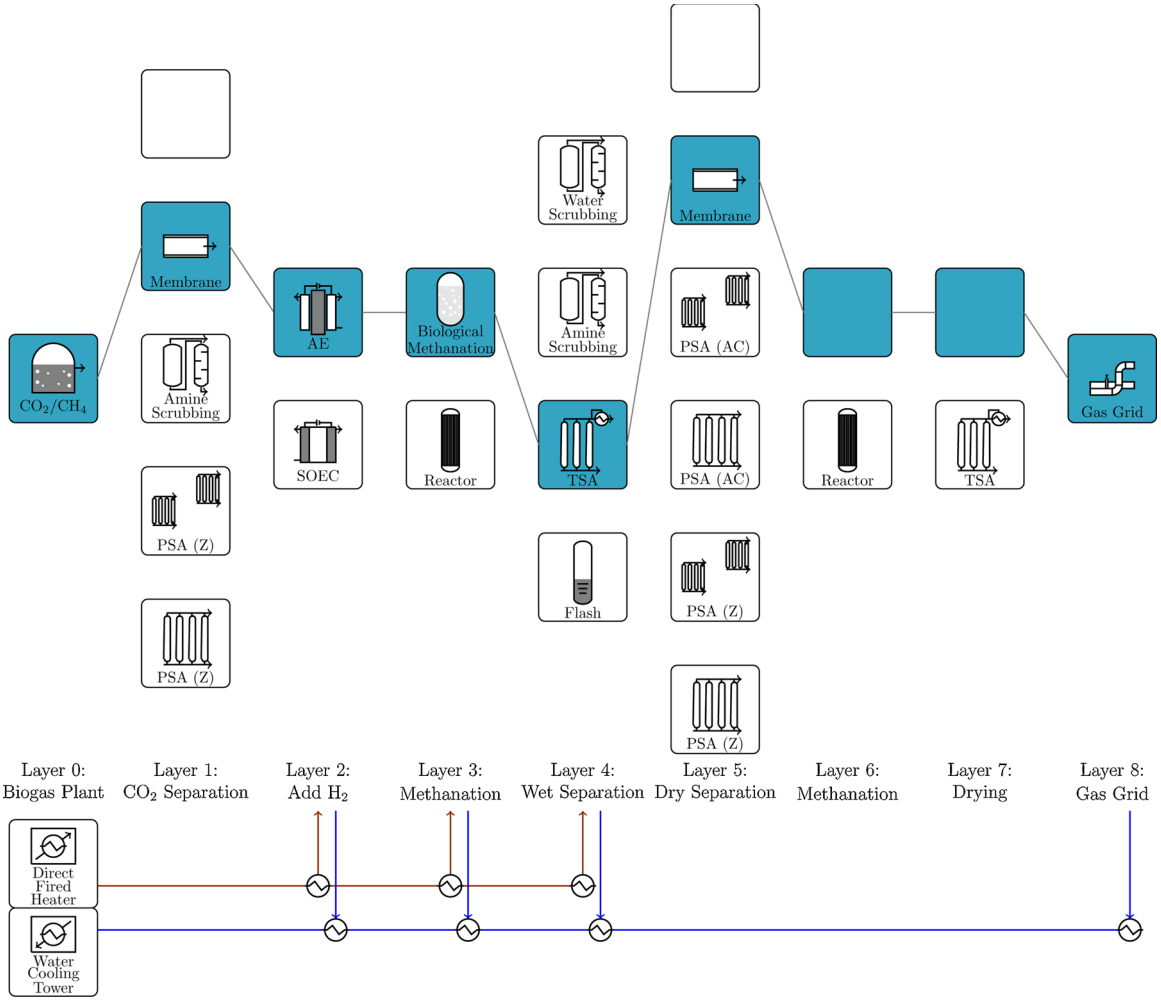

Fig. 13. Solution path: biomethanation with low CH_4 product concentration. The configuration is optimal in terms of efficiency for the choice of AE if a low concentration of methane can be produced by the bioreactor. Membrane separation is chosen twice in the process, prior and after methanation.

For the bioreactor BIO1 with a high concentration of methane in the output gas of 96%, the product gas does not need further purification apart from drying. Fig. 12 shows the corresponding process configuration. The bioreactor BIO2 produces gas with a concentration of 65% CH_4, which is not suitable for direct feeding to the gas grid. The result for this case shown in Fig. 13 includes additional purification via membrane separation. However, the second-best solution utilizing PSA instead of membrane separation was very close to this result (within 0.4% of the objective value). A more detailed analysis for this case is needed.

The processes using biological methanation show increased capital costs compared to the processes using catalytic methanation. The increase in cost is contributed to the increased cost of the biological methanation unit itself. However, capital costs of the heat integration network for the AE process are reduced significantly, as shown in Figs. 10 and 11 in terms of CAPEX and OPEX respectively. Combining the high efficiency of the SOEC with a high conversion rate in the bioreactor results in a large amount of product gas (SOEC BIO1). Nonetheless, the SOEC processes have a higher CAPEX per product in terms of LHV than the AE processes, as Fig. 10 shows. If the conversion rate is low (SOEC BIO2), a large quantity of gas is recycled from the membrane separation unit. This results in large mass flow rates within the process and high costs for compression and heat exchanger equipment.

4. Conclusions

We applied a superstructure optimization approach to power-to-methane processes, related to 12 different scenarios. The processes were optimized in terms of exergy efficiency, which unifies the contributions of electrical, heat, and chemical flows to one energetic value. Alternatively, the processes were optimized with respect to economic objectives CAPEX and TAC.

- The most efficient process with an efficiency of 65.8% utilizes SOEC for water electrolysis and includes heat integration within the process. The catalytic methanation was found to be a suitable heat source for preheating the steam for water electrolysis up to reactor temperature. However, an extensive heat exchanger network and the SOEC electrolyzer technology lead to high capital costs.
- The indirect heat integration, as included in the superstructure, showed a significant influence both on the process costs and efficiency, which was especially pronounced in the case of high-temperature electrolyzer, SOEC, where the catalytic methanation reactor can act as heat source for preheating of steam up to reactor temperature. Including internal heat integration increased the efficiency of processes with AE by 5%, while the efficiency of processes with SOEC increased by 7%.
- We showed, that the specification of the gas grid have an influence on the optimal process configuration. Increasing the threshold for feed of hydrogen to the gas grid reduces the number of necessary

unit operations.

Furthermore, we assessed the potential of substituting the conventional chemical methanation unit with a biological one.

- The downstream configuration of the biological methanation was found to be dependent on the expected methane concentration of the unit, and as shown in the analysis a membrane separation unit was preferred for a methane concentration of 65 mol% in the product gas. However, using other separation units such as pressure swing adsorption results in similar efficiency and cost, so that we cannot determine a clear best solution given the limited accuracy of the black box models.
- Process configurations with biological methanation have a limited potential for internal heat integration because of the lack of heat sources at higher temperatures. This results in decreased efficiency, especially for processes with SOEC.

Acknowledgements

This research was supported by the EU-program ERDF (European Regional Development Fund) of the German Federal State Saxony-Anhalt within the Research Center of Dynamic Systems (CDS).

Jennifer Uebbing is affiliated with the “International Max Planck Research School for Advanced Methods in Process and Systems Engineering – IMPRS ProEng” at the Max Planck Institute for Dynamics of Complex Technical Systems Magdeburg.

Funding by the German Federal Ministry of Education and Research, program “Mathematics for Innovations”, grant P2Chem, and by the European Research Council (ERC, grant agreement No 647573) under the European Union's Horizon 2020 research and innovation program is gratefully acknowledged by Sebastian Sager.

Kai Sundmacher received funding by the Deutsche Forschungsgemeinschaft (DFG, German Research Foundation) – Projektnummer 406914011 (Gefördert durch die Deutsche Forschungsgemeinschaft (DFG) – Projektnummer 406914011). We would like to thank Editage (www.editage.com) for English language editing.

Appendix A. Supplementary data

Supplementary data associated with this article can be found, in the online version, at https://doi.org/10.1016/j.jcou.2020.101228.

References

[1] H. Blanco, A. Faaij, A review at the role of storage in energy systems with a focus on power to gas and long-term storage, Renew. Sustain. Energy Rev. 81 (May 2017) (2018) 1049–1086.
[2] T.T. Vo, A. Xia, F. Rogan, D.M. Wall, J.D. Murphy, Sustainability assessment of large-scale storage technologies for surplus electricity using group multi-criteria decision analysis, Clean Technol. Environ. Policy 19 (3) (2017) 689–703.
[3] B. Castellani, A.M. Gambelli, E. Morini, B. Nastasi, A. Presciutti, M. Filipponi, A. Nicolini, F. Rossi, Experimental investigation on CO_2 methanation process for solar energy storage compared to CO_2-based methanol synthesis, Energies 10 (7) (2017) 1–13.
[4] P. Collet, E. Flottes, A. Favre, L. Raynal, H. Pierre, S. Capela, C. Peregrina, Techno-economic and life cycle assessment of methane production via biogas upgrading and power to gas technology, Appl. Energy 192 (2017) 282–295.
[5] M. Götz, J. Lefebvre, F. Mörs, A. McDaniel Koch, F. Graf, S. Bajohr, R. Reimert, T. Kolb, Renewable power-to-gas: a technological and economic review, Renew. Energy 85 (2016) 1371–1390.
[6] M. Bailera, P. Lisbona, L.M. Romeo, S. Espatolero, Power to Gas Projects Review: Lab, Pilot and Demo Plants for Storing Renewable Energy and CO_2, (2017).
[7] S. Rönsch, J. Schneider, S. Matthischke, M. Schlüter, M. Götz, J. Lefebvre, P. Prabhakaran, S. Bajohr, Review on methanation – from fundamentals to current projects, Fuel 166 (2016) 276–296.
[8] J. Bremer, P. Goyal, L. Feng, P. Benner, K. Sundmacher, POD-DEIM for efficient reduction of a dynamic 2D catalytic reactor model, Comput. Chem. Eng. 106 (2017) 777–784.
[9] A. Bensmann, R. Hanke-Rauschenbach, R. Heyer, F. Kohrs, D. Benndorf, U. Reichl, K. Sundmacher, Biological methanation of hydrogen within biogas plants: a model-based feasibility study, Appl. Energy 134 (2014) 413–425.
[10] F. Graf, A. Krajete, U. Schmack, Abschlussbericht Techno-ökonomische Studie zur biologischen Methanisierung bei Power-to-Gas-Konzepten, Deutscher Verein des Gas- und Wasserfaches e.V, 2014.
[11] A.H. Seifert, S. Rittmann, C. Herwig, Analysis of process related factors to increase volumetric productivity and quality of biomethane with *Methanothermobacter marburgensis*, Appl. Energy 132 (2014) 155–162.
[12] M.A. Voelklein, D. Rusmanis, J.D. Murphy, Biological methanation: strategies for in-situ and ex-situ upgrading in anaerobic digestion, Appl. Energy 235 (August 2018) (2019) 1061–1071.
[13] B. Castellani, S. Rinaldi, E. Morini, B. Nastasi, F. Rossi, Flue gas treatment by power-to-gas integration for methane and ammonia synthesis – energy and environmental analysis, Energy Convers. Manag. 171 (June) (2018) 626–634.
[14] J. Witte, A. Calbry-Muzyka, T. Wieseler, P. Hottinger, S.M. Biollaz, T.J. Schildhauer, Demonstrating direct methanation of real biogas in a fluidised bed reactor, Appl. Energy 240 (September 2018) (2019) 359–371.
[15] I. Ullah Khan, M. Hafiz Dzarfan Othman, H. Hashim, T. Matsuura, A.F. Ismail, M. Rezaei-DashtArzhandi, I. Wan Azelee, Biogas as a renewable energy fuel – a review of biogas upgrading, utilisation and storage, Energy Convers. Manag. 150 (May) (2017) 277–294.
[16] E. Giglio, F.A. Deorsola, M. Gruber, S.R. Harth, E.A. Morosanu, D. Trimis, S. Bensaid, R. Pirone, Power-to-gas through high temperature electrolysis and carbon dioxide methanation: reactor design and process modeling, Ind. Eng. Chem. Res. 57 (11) (2018) 4007–4018.
[17] G. Jeanmonod, L. Wang, S. Diethelm, F. Maréchal, J. Van herle, Trade-off designs of power-to-methane systems via solid-oxide electrolyzer and the application to biogas upgrading, Appl. Energy 247 (April) (2019) 572–581.
[18] S. de Oliveira, Exergy Production, Cost and Renewability, 2012.
[19] M. Shukuya, Theory and Applications in the Built Environment, (2012).
[20] I.E. Grossmann, Global Optimization in Engineering Design, vol. 9 of Nonconvex Optimization and its Applications, Springer US, Boston, MA, 1996.
[21] X. Hong, Z. Liao, B. Jiang, J. Wang, Y. Yang, Simultaneous optimization of heat-integrated water allocation networks, Appl. Energy 169 (2016) 395–407.
[22] E. Ahmetović, Z. Kravanja, Simultaneous synthesis of process water and heat exchanger networks, Energy 57 (2013) 236–250.
[23] I.E. Grossmann, P.A. Aguirre, M. Barttfeld, Optimal synthesis of complex distillation columns using rigorous models, Comput. Aided Chem. Eng. 18 (C) (2004) 53–74.
[24] J. Gong, F. You, Global optimization for sustainable design and synthesis of algae processing network for CO_2 mitigation and biofuel production using life cycle optimization, AIChE J. 60 (2014) 3195–3210.
[25] P. Linke, A. Kokossis, Attainable reaction and separation processes from a superstructure-based method, AIChE J. 49 (6) (2003) 1451–1470.
[26] I.E.G.Q. Chen, Recent developments and challenges in optimization-based process synthesis, Ann. Rev. Chem. Biomol. Eng. 8 (7) (2017) 249–283.
[27] F. Trespalacios, I.E. Grossmann, Chapter 24: Review of mixed-integer nonlinear optimization and generalized disjunctive programming applications in process systems engineering, Advances and Trends in Optimization with Engineering Applications (2017) 315–329.
[28] L. The Optimization Firm, “Baron | the optimization firm,” https://minlp.com/download (accessed: 10.02.2020).
[29] T. Achterberg, SCIP: Solving constraint integer programs, Math. Progr. Comput. 1 (1) (2009) 1–41.
[30] J. Kronqvist, D.E. Bernal, A. Lundell, I.E. Grossmann, A Review and Comparison of Solvers for Convex MINLP 20, Springer US, 2019.
[31] L.K. Rihko-Struckmann, A. Peschel, R. Hanke-Rauschenbach, K. Sundmacher, Assessment of methanol synthesis utilizing exhaust CO_2 for chemical storage of electrical energy, Ind. Eng. Chem. Res. 49 (21) (2010) 11073–11078.
[32] M. Gruber, P. Weinbrecht, L. Biffar, S. Harth, D. Trimis, J. Brabandt, O. Posdziech, R. Blumentritt, Power-to-gas through thermal integration of high-temperature steam electrolysis and carbon dioxide methanation – experimental results, Fuel Process. Technol. 181 (September) (2018) 61–74.
[33] F. Koschany, D. Schlereth, O. Hinrichsen, On the kinetics of the methanation of carbon dioxide on coprecipitated $NiAl(O)_x$, Appl. Catal. B: Environ. 181 (2016) 504–516.
[34] D. Stolten, V. Scherer, Transition to Renewable Energy Systems, Wiley-VCH Verlag GmbH & Co. KGaA, Weinheim, Germany, 2013 may.
[35] L.T. Biegler, I.E. Grossmann, W. Westerberg, Systematic Methods of Chemical Process Design, (1997).
[36] Zauba, “Export data and price of catalyst meth 134,” https://www.zauba.com/export-CATALYST+METH+134/hs-code-38151100/p-1-hs-code.html (accessed: 12.09.19).
[37] Alibaba, “Methanation Catalyst Suppliers and Manufacturers at alibaba.com,” https://www.alibaba.com/showroom/methanation-catalyst.html (accessed: 12.09.19).
[38] M.P. Hoffarth, T. Broeker, J. Schneider, Effect of N_2 on biological methanation in a continuous stirred-tank reactor with *Methanothermobacter marburgensis*, Fermentation 5 (3) (2019).

[39] J.-P. Peillex, M.-L. Fardeau, J.-P. Belaich, Growth of *Methanobacterium thermoautotrophicum* on H_2CO_2 high CH_4 productivities in continuous culture, Biomass 21 (1990) 315–321.
[40] H.A.E.S. Jee, N. Nishio, S. Nagai, Continuous CH_4 production from H_2 and CO_2 by *Methanobacterium thermoautotrophicum* in a fixed-bed reactor, 66(2) (1988) 235–238.
[41] F. Bauer, C. Hulteberg, T. Persson, D. Tamm, Biogas upgrading – review of commercial technologies, SGC 2013:270, Swedish Gas Technology Centre, SGC(June) (2013) 82.
[42] F. Ferella, A. Puca, G. Taglieri, L. Rossi, K. Gallucci, Separation of carbon dioxide for biogas upgrading to biomethane, J. Clean. Prod. 164 (2017) 1205–1218.
[43] R. Augelletti, M. Conti, M.C. Annesini, Pressure swing adsorption for biogas upgrading. A new process configuration for the separation of biomethane and carbon dioxide, J. Clean. Prod. 140 (2017) 1390–1398.
[44] J.H. Park, J.N. Kim, S.H. Cho, Performance analysis of four-bed H_2 PSA process using layered beds, AIChE J. 46 (4) (2000) 790–802.
[45] V. Kumar Gupta, M.G. Tuohy, Biofuel and Biorefinery Technologies 6 Biogas: Fundamentals, Process, and Operation, Springer, 2018.
[46] D. Schack, G. Liesche, K. Sundmacher, The FluxMax approach: simultaneous flux optimization and heat integration by discretization of thermodynamic state space illustrated on methanol synthesis process, Chem. Eng. Sci. (2020) 215.
[47] G. Liesche, D. Schack, K. Sundmacher, The FluxMax approach for simultaneous process synthesis and heat integration: production of hydrogen cyanide, AIChE J. (2019).
[48] EWK Kühlturm GmbH, https://ewk-kuehlturm.de/.
[49] J. Uebbing, L. Rihko-Struckmann, K. Sundmacher, Exergetic assessment of CO_2 methanation processes for the chemical storage of renewable energies, Appl. Energy (2019) 233–234.